

Dark Bondi Accretion Aided by Baryons and the Origin of JWST Little Red Dots

Wei-Xiang Feng,^{1,*} Hai-Bo Yu,^{2,†} and Yi-Ming Zhong^{3,‡}

¹*Department of Physics, Tsinghua University, Beijing 100084, China*

²*Department of Physics and Astronomy, University of California, Riverside, CA 92521, USA*

³*Department of Physics, City University of Hong Kong, Kowloon, Hong Kong SAR, China*

The gravothermal core collapse of self-interacting dark matter halos provides a compelling mechanism for seeding supermassive black holes in the early Universe. In this scenario, a small fraction of a halo, approximately 1% of its mass, collapses into a dense core, which could further evolve into a black hole. We demonstrate that this process can account for the origin of JWST little red dots (LRDs) observed at redshifts $z \sim 4\text{--}11$, where black holes with masses of $10^7 M_\odot$ can form within 500 Myr after the formation of host halos with masses of $10^9 M_\odot$. Even if the initial collapse region triggering general-relativistic instability has a mass on the order of one solar mass, the resulting seed can grow into an intermediate-mass black hole via Eddington accretion of baryonic gas. Subsequently, it can continue to grow into a supermassive black hole through dark Bondi accretion of dark matter particles. In this scenario, the majority of the black hole's mass originates from dark matter accretion rather than baryonic matter, naturally explaining the overmassive feature of LRDs.

Introduction. The origin of supermassive black holes (SMBHs) remains a mystery, particularly those found at high redshifts and associated with luminous quasars [1–7]. It is puzzling how a black hole could grow to a mass of $10^9 M_\odot$ when the Universe was only about 5% of its present age. In [8], we proposed a scenario to explain the origin of SMBHs associated with high-luminosity quasars, through the gravothermal collapse of self-interacting dark matter (SIDM) halos [9, 10]. As a self-gravitating system, an SIDM halo has a negative heat capacity, and its central region, corresponding to (0.1–1)% of the total mass, can collapse into an ultradense core, which can then further evolve into a black hole. We showed that the presence of compact central baryons can accelerate the onset of collapse and the self-interactions can dissipate the remnant angular momentum of the collapsed region. The collapse of massive halos of $10^{11} M_\odot$ at redshifts $z \gtrsim 10$ could produce a black hole with a mass of $10^8\text{--}10^9 M_\odot$; see also [11–14].

More recently, observations from the James Webb Space Telescope (JWST) have revealed compact active galactic nuclei at redshifts $z \sim 4\text{--}11$, hosting SMBHs with masses of $10^6\text{--}10^8 M_\odot$ [15–17]. These systems, referred to as little red dots (LRDs), exhibit unusually high black hole-to-stellar mass ratios of $\gtrsim 10^{-3}\text{--}10^{-1}$ [18], significantly larger than those observed in the local Universe [19]. This suggests that black holes in LRDs are overmassive relative to their host galaxies and likely originate from heavy seeds (e.g., [20]). Nevertheless, the detailed formation pathways of LRDs remain uncertain.

In this work, we explore the SIDM-based seeding mechanism for the formation of LRDs and show that they can arise from the gravothermal collapse of $10^9 M_\odot$ halos, with the central baryonic potential accelerating the

process. We address the crucial issue of how the entire collapsed central halo can evolve into a black hole, which was an assumption in earlier studies. To trigger general-relativistic instability, the 1D central velocity dispersion of dark matter particles must reach approximately $0.3c$ [9, 21]. Only a tiny fraction of the halo mass, on the order of $10^{-10}\text{--}10^{-8}$, can attain this condition following the trajectory of gravothermal evolution [9, 22].

For a $10^9 M_\odot$ halo relevant to the context of LRDs, the initial seed black hole mass is expected to be on the order of $1 M_\odot$. We show that such a solar-mass seed can grow to $10^7 M_\odot$ within 500 Myr through accretion. The initial growth phase is dominated by baryonic Eddington accretion, during which the black hole increases in mass from $1 M_\odot$ to $10^4 M_\odot$. After this stage, dark Bondi accretion becomes the dominant channel, efficiently consuming SIDM particles from the ultradense core and driving the black hole mass up to $10^7 M_\odot$. In this scenario, the resulting black hole is naturally overmassive, as its mass is built up primarily through dark matter accretion rather than baryonic processes, consistent with the observed feature of the LRDs.

We further demonstrate that Bondi accretion in the dark sector is not limited by a dark Eddington bound for viable SIDM particle models. Moreover, we show that the preferred range of dark matter self-interaction cross sections is consistent with SIDM models proposed to explain the diverse dark matter distributions observed in galaxies at low redshifts. Additionally, this scenario can be extended to cases where the initial black hole seed forms through the collapse of baryonic matter, such as pristine gas or stars. These findings open a new avenue for probing dark matter physics through observations of SMBHs; see also [23, 24] for complementary studies.

Gravothermal collapse timescale. We consider a Navarro-Frenk-White (NFW) halo formed at redshift z , and its density profile is given by $\rho_{\text{NFW}}(r) = \rho_s(r/r_s)^{-1}(1+r/r_s)^{-2}$ [25], where the scale density ρ_s

* wxfeng@mail.tsinghua.edu.cn

† haiboyu@ucr.edu

‡ yiming.zhong@cityu.edu.hk

and radius r_s are

$$\rho_s = \frac{200 \rho_c c_{200}^3}{3 f(c_{200})}, \quad r_s = \left(\frac{3 M_{200}}{800 \pi c_{200}^3 \rho_c} \right)^{1/3}, \quad (1)$$

respectively. M_{200} is the virial mass within the radius r_{200} , $c_{200} \equiv r_{200}/r_s$ is the halo concentration, $f(c_{200}) \equiv \ln(1 + c_{200}) - c_{200}/(1 + c_{200})$, and the critical density

$$\rho_c(z) = \frac{3H_0^2}{8\pi G} [\Omega_{m,0}(1+z)^3 + \Omega_\Lambda]. \quad (2)$$

We take $H_0 = 67.6 \text{ km/s/Mpc}$, $\Omega_{m,0} = 0.312$, and $\Omega_\Lambda = 0.688$ from Planck cosmology [26]. We can write $M_{200} = M_0 f(c_{200})$, where M_0 is the fiducial mass of the NFW halo $M_0 \equiv 4\pi \rho_s r_s^3$.

Assuming that dark matter self-interactions set to operate for the halo formed at redshift z , the core-collapse timescale can be estimated as [27]

$$\begin{aligned} t_{cc}(z) &= \frac{150}{C} \frac{t_0}{\rho_s r_s (\sigma/m)} \\ &\approx 495 \text{ Myr} \left(\frac{f(c_{200})}{f(3)} \right)^{3/2} \left(\frac{c_{200}}{3} \right)^{-7/2} \left(\frac{M_{200}}{10^9 M_\odot} \right)^{-1/3} \\ &\quad \times \left[\frac{\Omega_{m,0}(1+z)^3 + \Omega_\Lambda}{\Omega_{m,0}(1+10)^3 + \Omega_\Lambda} \right]^{-7/6} \left(\frac{\sigma/m}{150 \text{ cm}^2/\text{g}} \right)^{-1}, \end{aligned} \quad (3)$$

where C is a numerical coefficient and we take $C \simeq 0.75$ as calibrated from N -body simulations [28], $t_0 \equiv (4\pi G \rho_s)^{-1/2}$ is the fiducial timescale, and σ/m is the dark matter self-interacting cross section per unit particle mass, which should be interpreted as an effective cross section for the given halo mass in the context of velocity-dependent SIDM models [29, 30].

The halo concentration becomes insensitive to the halo mass at redshift $z \gtrsim 5$ and its median value asymptotes to $c_{200} \approx 3$ –4 [31]. As an estimate for LRDs, we consider a halo with a median concentration of $c_{200} = 3$ and a mass of $M_{200} \approx 10^9 M_\odot$ formed by $z = 10$, i.e., $t = 470 \text{ Myr}$ after the Big Bang. The required cross section is $\sigma/m \sim 150 \text{ cm}^2/\text{g}$ and $t_{cc} \sim 500 \text{ Myr}$. A black hole with mass $10^{-2} M_{200} \sim 10^7 M_\odot$ could form at $t \sim 970 \text{ Myr}$ ($z \sim 6$), assuming that the entire short-mean-free-path (SMFP) region evolves into the hole. If the halo has a relatively higher concentration, the cross section could be lower, e.g., $\sigma/m \approx 50 \text{ cm}^2/\text{g}$ for $c_{200} \approx 5$.

These conditions can be further relaxed after the effect of the central baryonic potential is included, as it accelerates the onset of gravothermal collapse [8, 28, 32–34]. To be concrete, we perform fluid simulations for an example: the LRD ID 61888 with a black hole mass of $1.66 \times 10^7 M_\odot$ at $z \approx 5.87$ [35]; see S.1 for details. Its stellar surface density is characterized by a Sérsic profile with index $n = 0.9$, half-light radius $R_* = 0.09 \text{ kpc}$, and stellar mass $M_* = 1.29 \times 10^8 M_\odot$. We fit the stellar distribution with the Plummer profile $\rho_B(r) = (3M_B/4\pi a^3) (1 + r^2/a^2)^{-5/2}$ with scale radius

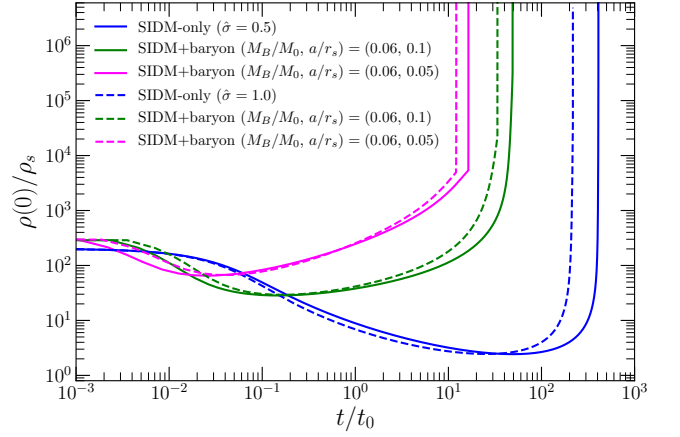


FIG. 1. Evolution of the normalized central density for the simulated halo without a baryonic potential (blue), and with a central Plummer baryonic potential assuming $(M_B/M_0, a/r_s) = (0.06, 0.1)$ (green) and $(0.06, 0.05)$ (magenta). Solid and dashed curves correspond to the fiducial self-interaction cross sections $\hat{\sigma} = 0.5$ and 1.0 , respectively.

$a = 0.1 \text{ kpc}$ and total mass $M_B = 1.4 \times 10^8 M_\odot$ to model the baryonic potential. We assume a halo at $z = 10$ with $M_{200} = 1.5 \times 10^9 M_\odot$ and $c_{200} = 3$, corresponding to $\rho_s \approx 1.5 \times 10^8 M_\odot/\text{kpc}^3$ and $r_s \approx 1.1 \text{ kpc}$. The fiducial time is $t_0 = 1/\sqrt{4\pi G \rho_s} \approx 10.9 \text{ Myr}$ and the fiducial mass $M_0 = 4\pi \rho_s r_s^3 \approx 2.4 \times 10^9 M_\odot$. Hence, $M_B/M_0 = 0.06$ and $a/r_s = 0.1$. Our simulations take two values for the fiducial cross section $\hat{\sigma} \equiv (\sigma/m) \rho_s r_s = 0.5$ and 1.0 , corresponding to $\sigma/m = 15 \text{ cm}^2/\text{g}$ and $30 \text{ cm}^2/\text{g}$, respectively.

Fig. 1 shows the evolution of the central density $\rho(0)/\rho_s$ of the simulated halo. For $\sigma/m = 15$ – $30 \text{ cm}^2/\text{g}$, the collapse timescale is $t_{cc} \approx 300$ – 500 Myr when the effect of central baryons is included (green), much shorter than that from the SIDM-only case $t_{cc} \approx 2$ – 4 Gyr (blue). The collapse timescale could be further shortened to 100 – 200 Myr if the baryon concentration is higher ($a/r_s = 0.05$; magenta). Our fluid simulations assume a static baryonic potential motivated by the observed stellar distribution. Hydrodynamical simulations of proto-galaxy formation indicate that the gas density profile may be steeper than the cored Plummer profile [36]. In [8], we showed that the effect with a power-law density profile for baryons, as motivated by [36], can reduce the core-collapse timescale by a factor of 100. Thus, the estimate shown in Fig. 1 may be considered conservative.

Using the Press–Schechter formalism [37], we estimate that the formation of $10^9 M_\odot$ halos by redshift $z \sim 10$ corresponds to a 3σ fluctuation above the mean density variance. In [8], we found that producing 10^8 – $10^9 M_\odot$ SMBHs at $z \sim 6$ – 7 requires the collapse of halos with masses in the range of 10^{11} – $10^{12} M_\odot$ at $z \sim 8$ – 11 , corresponding to 4 – 5σ peaks in the density field. Intriguingly, the existence of such rare halos is supported by JWST observations of massive galaxies with stellar masses $\gtrsim 10^{10}$ – $10^{11} M_\odot$ at $z \gtrsim 6$ – 7 [38, 39], whose host

halos are likely to lie in the 10^{11} – $10^{12} M_\odot$ range [40, 41]. Thus, the seeding mechanism could provide a unified explanation for the origin of SMBHs associated with both high- and low-luminosity quasars. Additionally, this seeding scenario favors a cross section in the range $\sigma/m \sim 10$ – $100 \text{ cm}^2/\text{g}$ for $10^9 M_\odot$ halos. This range is broadly consistent with SIDM models that have been shown to explain the dense substructures indicated by gravitational lensing systems [42–50] and stellar streams [51–53] through gravothermal collapse.

The initial black hole. In the estimate above, we have assumed that the black hole mass is set by the mass in the SMFP region M_{smfp} , which is characterized by the condition $Kn \equiv \lambda/H < 1$, where λ is the SIDM mean-free-path and H is the local Jeans length. From our fluid simulations, we find $M_{\text{smfp}} \sim 10^{-2} M_0$; see S.1 and also [8]. However, not all the mass in the SMFP region could collapse into a black hole instantaneously. In fact, the general-relativistic instability can only be triggered in the very central region, where the 1D velocity dispersion of SIDM particles reaches $\nu_{\text{GR}} \approx 0.3 c$ [9, 21]. The mass of this central region, denoted as M_{GR} , can be estimated using the scaling relation $M_{\text{GR}} \approx (\nu/\nu_{\text{GR}})^{2\alpha} M_{\text{smfp}}$ with $0.85 \lesssim \alpha \lesssim 1$, which is derived from the trajectory of gravothermal evolution [9, 22]. For halos with $M_{200} \sim 10^8$ – $10^{11} M_\odot$, $M_{\text{GR}}/M_{200} \approx 10^{-10}$ – 10^{-8} [22]. For LRDs, $M_{200} \sim 10^9 M_\odot$ and $M_{\text{GR}} \sim 1 M_\odot$. Note that $M_{200} = f(c_{200}) M_0 \sim M_0$, since $f(c_{200})$ is typically an $\mathcal{O}(1)$ factor.

The scaling relation relies on the extrapolation to the relativistic regime from fluid simulations. Here, we provide a complementary argument from the perspective of energy conservation [54]. Assuming the SMFP region itself is virialized, we have $K = |E| = -U/2$, where K is the kinetic energy, $|E|$ is the binding energy and U is the potential energy. $U = -0.6GM_{\text{smfp}}^2/r_{\text{smfp}}$, assuming a uniform density of the SMFP region, and hence $K = |E| = 0.3GM_{\text{smfp}}^2/r_{\text{smfp}}$. When the instability is triggered at the halo center, the associated binding energy is $0.035M_{\text{GR}}c^2$ [21]. Meanwhile, the binding energy of the remaining part of the SMFP region is $0.3GM_{\text{rem}}^2/r_{\text{rem}}$. From the condition of energy conservation, we have $0.035M_{\text{GR}}c^2 + 0.3GM_{\text{rem}}^2/r_{\text{rem}} = 0.3GM_{\text{smfp}}^2/r_{\text{smfp}}$, which is equal to the binding energy in magnitude. Therefore, we have $0.035M_{\text{GR}}c^2 \lesssim 0.3GM_{\text{smfp}}^2/r_{\text{smfp}}$, and

$$\frac{M_{\text{GR}}}{M_{\text{smfp}}} \lesssim 10 \times \left(\frac{10^{-2} r_s}{r_{\text{smfp}}} \right) \left(\frac{M_{\text{smfp}}}{10^{-2} M_0} \right) \frac{GM_0}{c^2 r_s}. \quad (4)$$

If $M_0 \approx 10^9 M_\odot$ and $r_s \approx 1 \text{ kpc}$ for LRDs, we obtain $M_{\text{GR}}/M_{\text{smfp}} \lesssim 10^{-7}$, corresponding to $M_{\text{GR}} \sim 1 M_\odot$. For $M_0 \approx 10^{12} M_\odot$ and $r_s \approx 10 \text{ kpc}$, we obtain $M_{\text{GR}} \sim 10^5 M_\odot$. These estimates are broadly consistent with those from [22]. Even if the initial seed mass is as small as $1 M_\odot$, it can still grow rapidly into an SMBH by accretion. In what follows, we first discuss dark Bondi accretion and then the role of baryonic Eddington accretion.

Dark Bondi accretion. Since dark matter in the SMFP region is in the hydrodynamic limit ($Kn < 1$), we apply the Bondi accretion [55–57] to model the initial seed accreting the surrounding SIDM particles

$$\dot{M}_{\text{Bon}} = 4\pi\lambda_s \frac{G^2 M^2}{a_\infty^3} \rho_\infty, \quad (5)$$

where the mass density $\rho_\infty = mn_\infty$ and sound speed a_∞ are evaluated at a distance r_∞ much larger than the Bondi radius $r_{\text{Bon}} = 2GM/a_\infty^2$. We take r_∞ to be the edge of the SMFP region. The accretion eigenvalue $\lambda_s = \lambda_s(\gamma)$ is an $\mathcal{O}(1)$ factor that depends on the adiabatic index γ of the accreted SIDM fluid, $\gamma = 4/3 + \sqrt{1 - 3\nu_\infty^2/c^2}/3$ [58], where ν_∞ denotes the 1D velocity dispersion at r_∞ and $\nu_\infty = a_\infty/\sqrt{\gamma} \ll c$. We take $\gamma \approx 5/3$, which gives $\lambda_s \approx 0.25$ [59].

Assuming ρ_∞ and a_∞ are nearly constant during the accretion process, the timescale is obtained by integrating of Bondi accretion rate, i.e.,

$$t_{\text{acc}} = \frac{a_\infty^3}{4\pi\lambda_s G^2 \rho_\infty} \left(\frac{1}{M_{\text{GR}}} - \frac{1}{M_{\text{smfp}}} \right). \quad (6)$$

At $r_\infty \sim r_{\text{smfp}} \sim 10^{-2} r_s$, the sound speed $a_\infty = \sqrt{\gamma} \nu_\infty$. We parametrize the conditions at r_∞ as $\rho_\infty = A \rho_s$ and $\nu_\infty = B \nu_0$, where $\nu_0 \equiv r_s \sqrt{4\pi G \rho_s}$ is a fiducial velocity. Thus, $a_\infty = \sqrt{\gamma} B \nu_0$. Since $M_{\text{GR}} \ll M_{\text{smfp}}$, we can neglect the term proportional to $1/M_{\text{smfp}}$ in Eq. 6 and express t_{acc} as

$$t_{\text{acc}} = 8.6 \left(\frac{B^3}{A} \right) \frac{M_0}{M_{\text{GR}}} t_0 \quad (7)$$

where $M_0 = 4\pi\rho_s r_s^3$ and $t_0 = 1/\sqrt{4\pi G \rho_s}$. For the case of LRDs, $M_0 \sim 10^9 M_\odot$, $t_0 \sim 11 \text{ Myr}$, $M_0/M_{\text{GR}} \sim 10^9$, and $B^3/A \sim 10^{-5}$ from our fluid simulations; see S.1, $t_{\text{acc}} \sim 10^3 \text{ Gyr}$, which is too long to be relevant. For $10^9 M_\odot$ SMBHs associated with high-luminosity quasars as studied in [8], $M_0 \sim 10^{12} M_\odot$, $t_0 \sim 15 \text{ Myr}$, $M_0/M_{\text{GR}} \sim 10^7$, and $B^3/A \sim 10^{-7}$. In this case, $t_{\text{acc}} \sim 129 \text{ Myr}$, which is comparable to the collapse timescale.

For the Bondi accretion to be valid, the Bondi radius must be smaller than the boundary radius of the SMFP region, i.e., $r_{\text{Bon}} < r_\infty$. We find that $r_{\text{Bon}} = 2GM/a_\infty^2 \lesssim (1.2/B^2)(M_{\text{smfp}}/M_0)r_s \approx (1.2 \times 10^{-2})(10^{-2})r_s$ in this scenario, which is smaller than $r_\infty \sim 10^{-2} r_s$. Thus, it is reasonable to treat the SIDM accretion from the SMFP region as a Bondi problem.

Baryonic Eddington accretion. Intriguingly, observations indicate that baryonic gas is abundant in LRDs [60]. In this section, we show that baryonic accretion plays a crucial role in enabling the seed black hole to achieve rapid early growth. The rate of Eddington accretion of baryonic gas is

$$\dot{M}_{\text{Edd}} = \left(\frac{1 - \epsilon}{\epsilon} \right) f_{\text{Edd}} \frac{4\pi GM}{(\sigma_{\text{rad}}/m)c}, \quad (8)$$

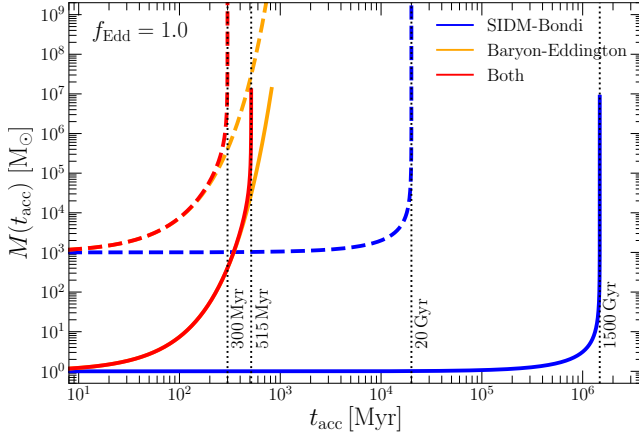


FIG. 2. Growth rate of the black hole mass due to dark Bondi accretion (blue), baryonic Eddington accretion (orange), and their combined contribution (red), shown for initial seed masses of $M_{\text{GR}} = 1 M_{\odot}$ (solid) and $10^3 M_{\odot}$ (dashed).

where ϵ is the radiative efficiency, f_{Edd} is the accretion efficiency, σ_{rad} is the cross section responsible for the radiation pressure. Combining Eqs. 5 and 8, we obtain the total accretion rate $\dot{M} = \dot{M}_{\text{Edd}} + \dot{M}_{\text{Bon}}$, which can be integrated to give the black hole mass as a function of time:

$$M(t_{\text{acc}}) = \frac{M_{\text{GR}} e^{t_{\text{acc}}/\tau}}{1 - \dot{M}_{\text{Bon}}/\dot{M}_{\text{Edd}}|_{M_{\text{GR}}} (e^{t_{\text{acc}}/\tau} - 1)}, \quad (9)$$

where $\tau \equiv [(\frac{1-\epsilon}{\epsilon}) f_{\text{Edd}} \frac{4\pi G}{(\sigma_{\text{rad}}/m)c}]^{-1}$ is the Salpeter time [61]. Taking $\epsilon = 0.1$, $\sigma_{\text{rad}}/m = 0.4 \text{ cm}^2/\text{g}$ for the Thomson cross section, and $f_{\text{Edd}} = 1$, we have $\tau = 50 \text{ Myr}$ and

$$\begin{aligned} \frac{\dot{M}_{\text{Bon}}}{\dot{M}_{\text{Edd}}}|_{M_{\text{GR}}} &= \lambda_s \left(\frac{\epsilon}{1-\epsilon} \right) \frac{\sigma_{\text{rad}}/m}{f_{\text{Edd}}} \frac{GM_{\text{GR}}}{a_{\infty}^3} \rho_{\infty} c \\ &= \lambda_s \left(\frac{\epsilon}{1-\epsilon} \right) \frac{\sigma_{\text{rad}}/m}{f_{\text{Edd}}} \left(\frac{A}{B^3} \right) \gamma^{-3/2} \frac{M_{\text{GR}}}{M_0} \rho_s c t_0 \end{aligned} \quad (10)$$

Because the Eddington accretion rate scales linearly with mass $\dot{M}_{\text{Edd}} \propto M$, whereas the Bondi accretion rate scales as $\dot{M}_{\text{Bon}} \propto M^2$, baryonic Eddington accretion dominates in the early growth phase when the seed mass is small as $\dot{M}_{\text{Bon}}/\dot{M}_{\text{Edd}}|_{M_{\text{GR}}} \ll 1$. However, as the black hole grows, dark Bondi accretion eventually takes over in a second phase, rapidly consuming the entire SMFP core once $e^{t_{\text{acc}}/\tau} \dot{M}_{\text{Bon}}/\dot{M}_{\text{Edd}}|_{M_{\text{GR}}} \sim \mathcal{O}(1)$.

In Fig. 2, we show the growth rate of the black hole mass due to dark Bondi accretion (blue), baryonic Eddington accretion (orange), and their combined contribution (red). For the LRD candidate (solid), we assume a halo of $M_{200} = 10^9 M_{\odot}$ with concentration $c_{200} = 3$ at $z = 10$. The initial seed mass is $M_{\text{GR}} = 1 M_{\odot}$, $A/B^3 = 10^5$, and $\dot{M}_{\text{Bon}}/\dot{M}_{\text{Edd}}|_{M_{\text{GR}}} f_{\text{Edd}} \approx 3.4 \times 10^{-5}$. For $f_{\text{Edd}} = 1$, baryonic accretion dominates the growth until the black hole reaches $\sim 10^4 M_{\odot}$. After that point,

dark Bondi accretion takes over, and the black hole quickly grows to $10^7 M_{\odot}$ within $\sim 500 \text{ Myr}$, much faster than 1500 Gyr it would require with dark accretion alone.

In this scenario, the majority of the black hole mass originates from SIDM particles in the SMFP region of the halo, rather than from baryonic matter. This may explain the overmassive feature of LRDs. Without dark Bondi accretion, the black hole could still grow to a mass of $10^7 M_{\odot}$ through baryonic Eddington accretion alone, albeit over a longer timescale. However, in this case, the seed would need to accrete on the order of $10^7 M_{\odot}$ of baryonic material. This could be in tension with the overmassive feature of LRDs, although the details depend on the initial baryonic content and the feedback processes during accretion.

In Fig. 2, we also show a case for more massive black holes, where we set $M_{\text{GR}} = 10^3 M_{\odot}$ in a halo formed at $z = 8$ with $M_{200} = 10^{12} M_{\odot}$ and $c_{200} = 3$. We use $A/B^3 = 10^7$, and $\dot{M}_{\text{Bon}}/\dot{M}_{\text{Edd}}|_{M_{\text{GR}}} f_{\text{Edd}} \approx 2.5 \times 10^{-3}$ [8]. Baryonic Eddington accretion dominates the black hole growth until the mass reaches approximately $10^6 M_{\odot}$. Then, dark Bondi accretion becomes the primary driver, and the black hole to grow to $10^9 M_{\odot}$ within 300 Myr . Such massive black holes could power the high-luminosity quasars observed at high redshifts [1–7].

Dark Eddington limit. When a black hole becomes sufficiently massive, its dark Bondi accretion rate could become Eddington-limited due to dark radiation pressure, i.e., $\dot{M}_{\text{Bon}}/\dot{M}_{\text{Edd}} \lesssim 1$ in Eq. 10, where \dot{M}_{Edd} now refers to dark matter particles rather than baryons. Consider a generic SIDM particle model consisting of a fermionic dark matter particle χ that couples to a dark mediator ϕ with a coupling constant g_{χ} (e.g., [62]). In this model, the self-scattering cross section $\chi\chi \rightarrow \chi\chi$ scales as $\sigma_{\chi\chi} \propto g_{\chi}^4 m_{\chi}^2/m_{\phi}^4$, where m_{χ} is the dark matter particle's mass and m_{ϕ} is the mediator's mass. Meanwhile, the cross section for dark Thomson-like scattering off the mediator, $\chi\phi \rightarrow \chi\phi$, scales as $\sigma_{\chi\phi} \propto g_{\chi}^4/m_{\chi}^2$ in the limit $m_{\phi} \ll m_{\chi}$.

For a viable SIDM model, the self-scattering cross section must be velocity-dependent across all halo mass scales from dwarfs to clusters, with an upper limit of $\sim 0.1 \text{ cm}^2/\text{g}$ inferred from cluster strong lensing ($M_{200} \sim 10^{15} M_{\odot}$) [63–65]. This indicates $m_{\phi}/m_{\chi} \lesssim 10^{-3}$ for the model. For Bondi accretion, the temperature near the black hole could reach $\gtrsim 0.1 m_{\chi} c^2$ [59], so the dark mediator ϕ would be populated in the plasma. Although dark radiation pressure can be generated by the $\chi\phi \rightarrow \chi\phi$ scattering process, the associated opacity is extremely suppressed: $\sigma_{\chi\phi}/\sigma_{\chi\chi} \sim (m_{\phi}/m_{\chi})^4 \sim 10^{-12}$. For $\sigma_{\chi\chi}/m \sim 10 \text{ cm}^2/\text{g}$, $\sigma_{\chi\phi}/m_{\chi} \sim 10^{-11} \text{ cm}^2/\text{g}$. Thus, from Eq. 10, we see that Bondi accretion of SIDM onto a black hole is not Eddington-limited for viable SIDM models.

Discussion. There are several aspects that warrant further improvement. Our estimates of the initial seed mass and the SMFP mass are primarily based on fluid simulations. However, recent studies suggest that the fluid approximation may break down during the late

stages of evolution—for instance, when the velocity dispersion becomes anisotropic [53, 66, 67]. At very late times, as the velocity dispersion increases significantly, dissipative processes associated with the mediator particle may also become important. More work is needed to assess the impact of these effects in the presence of a baryonic potential.

Moreover, our scenario can be extended to cases where the initial black hole seed forms through the collapse of baryonic matter, such as pristine gas or stars. For example, if a seed of one solar mass, composed of baryonic matter, resides at the center of a mildly collapsing SIDM halo, it can still grow into an SMBH via dark Bondi accretion, aided by baryonic Eddington accretion. In this extended scenario, the SIDM halo only needs to be in a mildly collapsing phase, thereby avoiding the potential complications associated with the late-stage collapse discussed above.

Conclusions. We have investigated the formation of the JWST LRDs in the SIDM framework, in which the central dark matter halo undergoes gravothermal collapse to form a seed black hole. Even if the initially collapsing region that triggers relativistic instability has a mass on the order of one solar mass, the resulting seed can grow into an intermediate-mass black hole via Eddington accretion of baryonic gas, and subsequently evolve into

an SMBH through dark Bondi accretion of SIDM particles. In this scenario, the majority of the black hole’s mass originates from SIDM accretion rather than baryonic matter, naturally explaining the overmassive feature of the LRDs. In the future, dedicated numerical simulations are needed to test dark Bondi accretion and other SIDM accretion processes [68, 69]. It will be important to investigate the predicted population of LRDs within this framework [23] and explore the associated gravitational wave signatures [24].

The code used to model SIDM gravothermal evolution in the presence of a static baryonic potential is publicly available at <https://github.com/ymzhong/gravothermal>.

We thank Moritz Fischer, Fangzhou Jiang, Manoj Kaplinghat, and Pranjal Ralegankar for useful discussions. WXF was supported by Tsinghua’s Shuimu Scholar Fellowship and the China Postdoctoral Science Foundation under Grant No. 2024M761594. HBY was supported by the U.S. Department of Energy under Grant No. DE-SC0008541. YZ was supported by the GRF grant 11302824 from the Hong Kong Research Grants Council. This project was made possible through the support of Grant 63599 from the John Templeton Foundation (HBY). The opinions expressed in this publication are those of the authors and do not necessarily reflect the views of the John Templeton Foundation.

-
- [1] D. J. Mortlock, S. J. Warren, B. P. Venemans, M. Patel, P. C. Hewett, R. G. McMahon, C. Simpson, T. Theuns, S. P. Allanson, K. M. Blundell, P. R. Cannon, C. J. Conselice, M. J. Cowley, S. Dye, S. A. Eales, D. L. Edmunds, S. L. Ellison, S. L. Finkelstein, M. Fumagalli, J. A. Gorge, E. A. Gonzalez-Solares, V. Gonzalez-Perez, N. C. Hambly, M. Hastie, M. J. Irwin, K. Kuijken, I. R. Parry, J. A. Peacock, S. Phillipps, A. Pontzen, B. Rodriguez-del Pino, J. Savidge, M. A. Thomson, B. Vinter, I. Waddington, C. J. Walcher, and J. M. Weatherley, “Detection of a $z=7.08$ quasar in the IRAC Dark Field,” *Nature* **474** (2011) 616–619, [arXiv:1106.6088 \[astro-ph.CO\]](#).
 - [2] X.-B. Wu, F. Wang, X. Fan, W. Yi, W. Zuo, F. Bian, L. Jiang, I. D. McGreer, R. Wang, J. Yang, Y. Xue, and G. Ai, “An ultraluminous quasar with a twelve-billion-solar-mass black hole at redshift 6.30,” *Nature* **518** (2015) 512–515, [arXiv:1502.07418 \[astro-ph.GA\]](#).
 - [3] E. Banados *et al.*, “An 800-million-solar-mass black hole in a significantly neutral Universe at redshift 7.5,” *Nature* **553** no. 7689, (2018) 473–476, [arXiv:1712.01860 \[astro-ph.GA\]](#).
 - [4] Y. Matsuoka, T. Izumi, M. Onoue, T. Nagao, N. Kashikawa, M. Imanishi, K. Kawara, S. Kim, J. D. Silverman, J. Tang, and Y. Toba, “Discovery of a Low-Luminosity Quasar at $z > 7$,” *Astrophys. J. Lett.* **872** (2019) L2, [arXiv:1901.10487 \[astro-ph.GA\]](#).
 - [5] F. Wang, X. Fan, J. Yang, F. Bian, L. Jiang, J.-T. Li, J.-G. Li, R. Wang, X.-B. Wu, and M. Yue, “A Luminous Quasar at Redshift $z = 7.54$,” *Astrophys. J. Lett.* **869** (2018) L9, [arXiv:1810.11925 \[astro-ph.GA\]](#).
 - [6] J. Yang, X. Fan, X. Ding, N. Kashikawa, F. Wang, F. Bian, L. Jiang, M. Onoue, B. P. Venemans, E. Banados, X.-B. Wu, M. Yue, Y. Gong, J. Huang, J.-G. Li, X. Liu, and B. Rosenwasser, “A Luminous Quasar at Redshift 7.642,” *Astrophys. J. Lett.* **907** (2021) L1, [arXiv:2101.03179 \[astro-ph.GA\]](#).
 - [7] A. Bogdan *et al.*, “Evidence for heavy-seed origin of early supermassive black holes from a $z \approx 10$ X-ray quasar,” *Nature Astron.* **8** no. 1, (2024) 126–133, [arXiv:2305.15458 \[astro-ph.GA\]](#).
 - [8] W.-X. Feng, H.-B. Yu, and Y.-M. Zhong, “Seeding Supermassive Black Holes with Self-interacting Dark Matter: A Unified Scenario with Baryons,” *Astrophys. J. Lett.* **914** no. 2, (2021) L26, [arXiv:2010.15132 \[astro-ph.CO\]](#).
 - [9] S. Balberg and S. L. Shapiro, “Gravothermal collapse of selfinteracting dark matter halos and the origin of massive black holes,” *Phys. Rev. Lett.* **88** (2002) 101301, [arXiv:astro-ph/0111176](#).
 - [10] S. Balberg, S. L. Shapiro, and S. Inagaki, “Selfinteracting dark matter halos and the gravothermal catastrophe,” *Astrophys. J.* **568** (2002) 475–487, [arXiv:astro-ph/0110561](#).
 - [11] J. Pollack, D. N. Spergel, and P. J. Steinhardt, “Supermassive Black Holes from Ultra-Strongly Self-Interacting Dark Matter,” *Astrophys. J.* **804** no. 2, (2015) 131, [arXiv:1501.00017 \[astro-ph.CO\]](#).
 - [12] J. Choquette, J. M. Cline, and J. M. Cornell, “Early formation of supermassive black holes via dark matter self-interactions,” *JCAP* **07** (2019) 036,

- [arXiv:1812.05088 \[astro-ph.CO\]](#).
- [13] H. Xiao, X. Shen, P. F. Hopkins, and K. M. Zurek, “SMBH seeds from dissipative dark matter,” *JCAP* **07** (2021) 039, [arXiv:2103.13407 \[astro-ph.CO\]](#).
 - [14] T. Meshveliani, J. Zavala, and M. R. Lovell, “Gravothermal collapse of self-interacting dark matter halos as the origin of intermediate mass black holes in Milky Way satellites,” *Phys. Rev. D* **107** no. 8, (2023) 083010, [arXiv:2210.01817 \[astro-ph.GA\]](#).
 - [15] D. D. Kocevski *et al.*, “Hidden Little Monsters: Spectroscopic Identification of Low-Mass, Broad-Line AGN at $z > 5$ with CEERS,” *Astrophys. J. Lett.* **954** no. 1, (2023) L4, [arXiv:2302.00012 \[astro-ph.GA\]](#).
 - [16] Y. Harikane *et al.*, “A JWST/NIRSpec First Census of Broad-Line AGNs at $z = 4$ –7: Detection of 10 Faint AGNs with $M_{\text{BH}} \sim 10^6$ – $10^8 M_{\odot}$ and Their Host Galaxy Properties,” *Astrophys. J.* **959** no. 1, (2023) 39, [arXiv:2303.11946 \[astro-ph.GA\]](#).
 - [17] J. Matthee *et al.*, “Little Red Dots: An Abundant Population of Faint Active Galactic Nuclei at $z \sim 5$ Revealed by the EIGER and FRESCO JWST Surveys,” *Astrophys. J.* **963** no. 2, (2024) 129, [arXiv:2306.05448 \[astro-ph.GA\]](#).
 - [18] F. Pacucci, B. Nguyen, S. Carniani, R. Maiolino, and X. Fan, “JWST CEERS and JADES Active Galaxies at $z = 4$ –7 Violate the Local M_{\bullet} – M_{\star} Relation at $>3\sigma$: Implications for Low-mass Black Holes and Seeding Models,” *Astrophys. J. Lett.* **957** no. 1, (2023) L3, [arXiv:2308.12331 \[astro-ph.GA\]](#).
 - [19] J. Kormendy and L. C. Ho, “Coevolution (Or Not) of Supermassive Black Holes and Host Galaxies,” *Ann. Rev. Astron. Astrophys.* **51** (2013) 511–653, [arXiv:1304.7762 \[astro-ph.CO\]](#).
 - [20] P. Natarajan, F. Pacucci, A. Ricarte, A. Bogdan, A. D. Goulding, and N. Cappelluti, “First Detection of an Overmassive Black Hole Galaxy UHZ1: Evidence for Heavy Black Hole Seed Formation from Direct Collapse,” *Astrophys. J. Lett.* **960** no. 1, (2024) L1, [arXiv:2308.02654 \[astro-ph.HE\]](#).
 - [21] W.-X. Feng, H.-B. Yu, and Y.-M. Zhong, “Dynamical instability of collapsed dark matter halos,” *JCAP* **05** no. 05, (2022) 036, [arXiv:2108.11967 \[astro-ph.CO\]](#).
 - [22] S. Gad-Nasr, K. K. Boddy, M. Kaplinghat, N. J. Outmezguine, and L. Sagunski, “On the late-time evolution of velocity-dependent self-interacting dark matter halos,” *JCAP* **05** (2024) 131, [arXiv:2312.09296 \[astro-ph.GA\]](#).
 - [23] F. Jiang, Z. Jia, H. Zheng, L. C. Ho, K. Inayoshi, X. Shen, M. Vogelsberger, and W.-X. Feng, “Formation of the Little Red Dots from the Core-collapse of Self-interacting Dark Matter Halos,” [arXiv:2503.23710 \[astro-ph.GA\]](#).
 - [24] T. Shen, X. Shen, H. Xiao, M. Vogelsberger, and F. Jiang, “Massive Black Holes Seeded by Dark Matter – Implications for Little Red Dots and Gravitational Wave Signatures,” [arXiv:2504.00075 \[astro-ph.GA\]](#).
 - [25] J. F. Navarro, C. S. Frenk, and S. D. M. White, “A Universal density profile from hierarchical clustering,” *Astrophys. J.* **490** (1997) 493–508, [arXiv:astro-ph/9611107](#).
 - [26] Planck Collaboration, N. Aghanim *et al.*, “Planck 2018 results. VI. Cosmological parameters,” *Astron. Astrophys.* **641** (2020) A6, [arXiv:1807.06209 \[astro-ph.CO\]](#). [Erratum: *Astron. Astrophys.* 652, C4 (2021)].
 - [27] R. Essig, S. D. McDermott, H.-B. Yu, and Y.-M. Zhong, “Constraining Dissipative Dark Matter Self-Interactions,” *Phys. Rev. Lett.* **123** no. 12, (2019) 121102, [arXiv:1809.01144 \[hep-ph\]](#).
 - [28] Y.-M. Zhong, D. Yang, and H.-B. Yu, “The impact of baryonic potentials on the gravothermal evolution of self-interacting dark matter haloes,” *Mon. Not. Roy. Astron. Soc.* **526** no. 1, (2023) 758–770, [arXiv:2306.08028 \[astro-ph.CO\]](#).
 - [29] D. Yang and H.-B. Yu, “Gravothermal evolution of dark matter halos with differential elastic scattering,” *JCAP* **09** (2022) 077, [arXiv:2205.03392 \[astro-ph.CO\]](#).
 - [30] D. Yang, E. O. Nadler, and H.-B. Yu, “Strong Dark Matter Self-interactions Diversify Halo Populations within and surrounding the Milky Way,” *Astrophys. J.* **949** no. 2, (2023) 67, [arXiv:2211.13768 \[astro-ph.GA\]](#).
 - [31] T. Ishiyama *et al.*, “The Uchuu simulations: Data Release 1 and dark matter halo concentrations,” *Mon. Not. Roy. Astron. Soc.* **506** no. 3, (2021) 4210–4231, [arXiv:2007.14720 \[astro-ph.CO\]](#).
 - [32] O. D. Elbert, J. S. Bullock, M. Kaplinghat, S. Garrison-Kimmel, A. S. Graus, and M. Rocha, “A Testable Conspiracy: Simulating Baryonic Effects on Self-Interacting Dark Matter Halos,” *Astrophys. J.* **853** no. 2, (2018) 109, [arXiv:1609.08626 \[astro-ph.GA\]](#).
 - [33] O. Sameie, M. Boylan-Kolchin, R. Sanderson, D. Varga, P. F. Hopkins, A. Wetzel, J. Bullock, A. Graus, and V. H. Robles, “The central densities of Milky Way-mass galaxies in cold and self-interacting dark matter models,” *Mon. Not. Roy. Astron. Soc.* **507** no. 1, (2021) 720–729, [arXiv:2102.12480 \[astro-ph.GA\]](#).
 - [34] G. Despali, L. Moscardini, D. Nelson, A. Pillepich, V. Springel, and M. Vogelsberger, “Introducing the AIDA-TNG project: Galaxy formation in alternative dark matter models,” *Astron. Astrophys.* **697** (2025) A213, [arXiv:2501.12439 \[astro-ph.CO\]](#).
 - [35] R. Maiolino *et al.*, “JADES - The diverse population of infant black holes at $4 < z < 11$: Merging, tiny, poor, but mighty,” *Astron. Astrophys.* **691** (2024) A145, [arXiv:2308.01230 \[astro-ph.GA\]](#).
 - [36] J. H. Wise, M. J. Turk, and T. Abel, “Resolving the Formation of Protogalaxies. II. Central Gravitational Collapse,” *Astrophys. J.* **682** (2008) 745, [arXiv:0710.1678 \[astro-ph\]](#).
 - [37] W. H. Press and P. Schechter, “Formation of galaxies and clusters of galaxies by selfsimilar gravitational condensation,” *Astrophys. J.* **187** (1974) 425–438.
 - [38] I. Labbé, P. van Dokkum, E. Nelson, R. Bezanson, K. A. Suess, J. Leja, G. Brammer, K. Whitaker, E. Mathews, M. Stefanon, and B. Wang, “A population of red candidate massive galaxies 600 Myr after the Big Bang,” *Nature* **616** no. 7956, (2023) 266–269, [arXiv:2207.12446 \[astro-ph.GA\]](#).
 - [39] M. Xiao, P. A. Oesch, D. Elbaz, L. Bing, E. J. Nelson, A. Weibel, G. D. Illingworth, P. van Dokkum, R. P. Naidu, E. Daddi, R. J. Bouwens, J. Matthee, S. Wuyts, J. Chisholm, G. Brammer, M. Dickinson, B. Magnelli, L. Leroy, D. Schaerer, T. Herard-Demanche, S. Lim, L. Barrufet, R. Endsley, Y. Fudamoto, C. Gómez-Guijarro, R. Gottumukkala, I. Labbé, D. Magee, D. Marchesini, M. Maseda, Y. Qin, N. A.

- Reddy, A. Shapley, I. Shivaee, M. Shuntov, M. Stefanon, K. E. Whitaker, and J. S. B. Wyithe, “Accelerated formation of ultra-massive galaxies in the first billion years,” *Nature* **635** no. 8038, (2024) 311–315, [arXiv:2309.02492](#).
- [40] M. Boylan-Kolchin, “Stress testing Λ CDM with high-redshift galaxy candidates,” *Nature Astron.* **7** no. 6, (2023) 731–735, [arXiv:2208.01611 \[astro-ph.CO\]](#).
- [41] E. O. Nadler, A. Benson, T. Driskell, X. Du, and V. Gluscevic, “Growing the first galaxies’ merger trees,” *Mon. Not. Roy. Astron. Soc.* **521** no. 3, (2023) 3201–3220, [arXiv:2212.08584 \[astro-ph.GA\]](#).
- [42] S. Vegetti, L. V. E. Koopmans, A. Bolton, T. Treu, and R. Gavazzi, “Detection of a Dark Substructure through Gravitational Imaging,” *Mon. Not. Roy. Astron. Soc.* **408** (2010) 1969, [arXiv:0910.0760 \[astro-ph.CO\]](#).
- [43] Q. E. Minor, S. Gad-Nasr, M. Kaplinghat, and S. Vegetti, “An unexpected high concentration for the dark substructure in the gravitational lens SDSSJ0946+1006,” *Mon. Not. Roy. Astron. Soc.* **507** no. 2, (2021) 1662–1683, [arXiv:2011.10627 \[astro-ph.GA\]](#).
- [44] E. O. Nadler, D. Yang, and H.-B. Yu, “A Self-interacting Dark Matter Solution to the Extreme Diversity of Low-mass Halo Properties,” *Astrophys. J. Lett.* **958** no. 2, (2023) L39, [arXiv:2306.01830 \[astro-ph.GA\]](#).
- [45] G. Despali, F. M. Heinze, C. D. Fassnacht, S. Vegetti, C. Spingola, and R. Klessen, “Detecting low-mass haloes with strong gravitational lensing II: constraints on the density profiles of two detected subhaloes,” [arXiv:2407.12910 \[astro-ph.CO\]](#).
- [46] W. J. R. Enzi, C. M. Krawczyk, D. J. Ballard, and T. E. Collett, “The overconcentrated dark halo in the strong lens SDSS J0946+1006 is a subhalo: evidence for self interacting dark matter?,” [arXiv:2411.08565 \[astro-ph.CO\]](#).
- [47] E. O. Nadler, D. Kong, D. Yang, and H.-B. Yu, “SIDM Concerto: Compilation and Data Release of Self-interacting Dark Matter Zoom-in Simulations,” [arXiv:2503.10748 \[astro-ph.CO\]](#).
- [48] M. Tajalli, S. Vegetti, C. M. O’Riordan, S. D. M. White, C. D. Fassnacht, D. M. Powell, J. P. McKean, and G. Despali, “SHARP – IX. The dense, low-mass perturbers in B1938+666 and J0946+1006: implications for cold and self-interacting dark matter,” [arXiv:2505.07944 \[astro-ph.CO\]](#).
- [49] S. Li *et al.*, “The ‘Little Dark Dot’: Evidence for Self-Interacting Dark Matter in the Strong Lens SDSSJ0946+1006?,” [arXiv:2504.11800 \[astro-ph.GA\]](#).
- [50] Q. He *et al.*, “Not so dark, not so dense: an alternative explanation for the lensing subhalo in SDSSJ0946+1006,” [arXiv:2506.07978 \[astro-ph.CO\]](#).
- [51] A. Bonaca, D. W. Hogg, A. M. Price-Whelan, and C. Conroy, “The Spur and the Gap in GD-1: Dynamical evidence for a dark substructure in the Milky Way halo,” [arXiv:1811.03631 \[astro-ph.GA\]](#).
- [52] X. Zhang, H.-B. Yu, D. Yang, and E. O. Nadler, “The GD-1 Stellar Stream Perturber as a Core-collapsed Self-interacting Dark Matter Halo,” *Astrophys. J. Lett.* **978** no. 2, (2025) L23, [arXiv:2409.19493 \[astro-ph.GA\]](#).
- [53] M. S. Fischer, H.-B. Yu, and K. Dolag, “Accurately simulating core-collapse self-interacting dark matter halos,” [arXiv:2506.06269 \[astro-ph.CO\]](#).
- [54] P. Ralegankar, D. Perri, and T. Kobayashi, “Gravothermalizing into primordial black holes, boson stars, and cannibal stars,” [arXiv:2410.18948 \[astro-ph.CO\]](#).
- [55] H. Bondi and F. Hoyle, “On the Mechanism of Accretion by Stars,” *Mon. Not. Roy. Astron. Soc.* **104** no. 5, (1944) 273–282.
- [56] H. Bondi, “Spherically symmetrical models in general relativity,” *Mon. Not. Roy. Astron. Soc.* **107** (1947) 410–425.
- [57] H. Bondi, “On spherically symmetrical accretion,” *Mon. Not. Roy. Astron. Soc.* **112** (1952) 195.
- [58] W.-X. Feng, “Gravothermal phase transition, black holes and space dimensionality,” *Phys. Rev. D* **106** no. 4, (2022) L041501, [arXiv:2207.14317 \[gr-qc\]](#).
- [59] S. L. Shapiro and S. A. Teukolsky, *Black holes, white dwarfs, and neutron stars: The physics of compact objects*. John Wiley & Sons, 1983.
- [60] R. P. Naidu *et al.*, “A ‘Black Hole Star’ Reveals the Remarkable Gas-Enshrouded Hearts of the Little Red Dots,” [arXiv:2503.16596 \[astro-ph.GA\]](#).
- [61] E. E. Salpeter, “Accretion of Interstellar Matter by Massive Objects,” *Astrophys. J.* **140** (1964) 796–800.
- [62] S. Tulin and H.-B. Yu, “Dark Matter Self-interactions and Small Scale Structure,” *Phys. Rept.* **730** (2018) 1–57, [arXiv:1705.02358 \[hep-ph\]](#).
- [63] M. Kaplinghat, S. Tulin, and H.-B. Yu, “Dark Matter Halos as Particle Colliders: Unified Solution to Small-Scale Structure Puzzles from Dwarfs to Clusters,” *Phys. Rev. Lett.* **116** no. 4, (2016) 041302, [arXiv:1508.03339 \[astro-ph.CO\]](#).
- [64] L. Sagunski, S. Gad-Nasr, B. Colquhoun, A. Robertson, and S. Tulin, “Velocity-dependent Self-interacting Dark Matter from Groups and Clusters of Galaxies,” *JCAP* **01** (2021) 024, [arXiv:2006.12515 \[astro-ph.CO\]](#).
- [65] K. E. Andrade, J. Fuson, S. Gad-Nasr, D. Kong, Q. Minor, M. G. Roberts, and M. Kaplinghat, “A stringent upper limit on dark matter self-interaction cross-section from cluster strong lensing,” *Mon. Not. Roy. Astron. Soc.* **510** no. 1, (2021) 54–81, [arXiv:2012.06611 \[astro-ph.CO\]](#).
- [66] J. Gurian and S. May, “Core Collapse Beyond the Fluid Approximation: The Late Evolution of Self-Interacting Dark Matter Halos,” [arXiv:2505.15903 \[astro-ph.CO\]](#).
- [67] M. Kamionkowski, K. Sigurdson, and O. Slone, “Numerical evolution of self-gravitating halos of self-interacting dark matter,” [arXiv:2506.04334 \[astro-ph.CO\]](#).
- [68] V. M. Sabarish, M. Brüggen, K. Schmidt-Hoberg, and M. S. Fischer, “Accretion of self-interacting dark matter onto supermassive black holes,” [arXiv:2505.14779 \[astro-ph.CO\]](#).
- [69] W.-X. Feng, A. Parisi, C.-S. Chen, and F.-L. Lin, “Self-interacting dark scalar spikes around black holes via relativistic Bondi accretion,” *JCAP* **08** no. 08, (2022) 032, [arXiv:2112.05160 \[astro-ph.HE\]](#).

— Supplemental Material —

Dark Bondi Accretion Aided by Baryons and the Origin of JWST Little Red Dots

Wei-Xiang Feng, Hai-Bo Yu, and Yi-Ming Zhong

Appendix S.1: Gravitational Evolution of SIDM halos

In our fluid simulations, we follow the procedure outlined in Refs. [8, 27, 28] to study the gravothermal evolution of an SIDM halo under the influence of a baryonic potential. The simulation code is publicly available at <https://github.com/ymzhong/gravothermal>.

The evolution of the halo can be described by the following equations

$$\begin{aligned} \frac{\partial M}{\partial r} &= 4\pi r^2 \rho, \quad \frac{\partial(\rho\nu^2)}{\partial r} = -\frac{G(M + M_B)\rho}{r^2}, \\ \frac{\partial L}{\partial r} &= -4\pi\rho r^2 \nu^2 D_t \ln \frac{\nu^3}{\rho}, \quad \frac{L}{4\pi r^2} = -\kappa \frac{\partial(m\nu^2)}{k_B \partial r}, \end{aligned} \quad (\text{S.1-1})$$

where M, ρ, ν , and L are enclosed dark matter mass, density, 1D velocity dispersion, and luminosity profiles, respectively, and they are dynamical variables and evolve with time; $M_B(r)$ is the mass profile of baryons; k_B is the Boltzmann constant, G is the Newton constant, and D_t denotes the Lagrangian time derivative. Heat conductivity of the dark matter fluid is given by $\kappa = (\kappa_{\text{lmp}}^{-1} + \kappa_{\text{smfp}}^{-1})^{-1}$, where $\kappa_{\text{lmp}} \approx 0.27C\rho\nu^3\sigma k_B/(Gm^2)$ and $\kappa_{\text{smfp}} \approx 2.1\nu k_B/\sigma$ denote conductivity in the long- and short-mean-free-path regimes, respectively, and $C \simeq 0.75$ as calibrated from N -body simulations. In the short-mean-free-path regime, heat conduction can be characterized by the self-interaction mean free path $\lambda = 1/(\sigma/m)$ and $Kn = \lambda/H < 1$, where $H = \nu/\sqrt{4\pi G\rho}$ is the scale height. In the long-mean-free-path regime, it is characterized by H and $Kn > 1$.

Assuming an initial halo concentration c_{200} with the given M_{200} and cosmic redshift z , we translate to the scale density ρ_s and radius r_s in the NFW halo profile

$$\rho_{\text{NFW}}(r) = \frac{\rho_s}{(r/r_s)(1 + r/r_s)^2}. \quad (\text{S.1-2})$$

We then normalize all physical quantities using ρ_s , r_s , and their combinations, including the fiducial time $t_0 \equiv 1/\sqrt{4\pi G\rho_s}$, fiducial mass $M_0 \equiv 4\pi\rho_s r_s^3$, and fiducial velocity $\nu_0 \equiv r_s\sqrt{4\pi G\rho_s}$, for implementation in the simulation.

We use a Plummer profile to model the baryon distribution in LRDs,

$$\rho_B(r) = \frac{3M_B}{4\pi a^3} \left(1 + \frac{r^2}{a^2}\right)^{-5/2}, \quad (\text{S.1-3})$$

where a and M_B are the scale radius and mass of the profile, respectively. We have checked that the Plummer profile provides a good approximation to the stellar distribution of the LRDs characterized by the Sérsic profile. The parameters relevant to the baryons are M_B/M_0 and a/r_s in the simulation.

Fig. 3 shows the density (top left), the ratio ρ/ν^3 (top right), the Knudsen number (bottom left), and the radius (bottom right) as functions of enclosed mass at different stages of gravothermal collapse, with (solid red) and without (dashed blue) including the baryonic potential. The dotted vertical lines mark the boundary of the short mean free path region, defined by $Kn = 1$. In the top left panel, the dash-dotted curve shows the baryon density profile. The simulation assumes $M_B/M_0 = 0.06$, $a/r_s = 0.1$, and $\hat{\sigma} = (\sigma/m)\rho_s r_s = 0.5$. Fig. 4 shows similar results, but for $\hat{\sigma} = 1.0$.

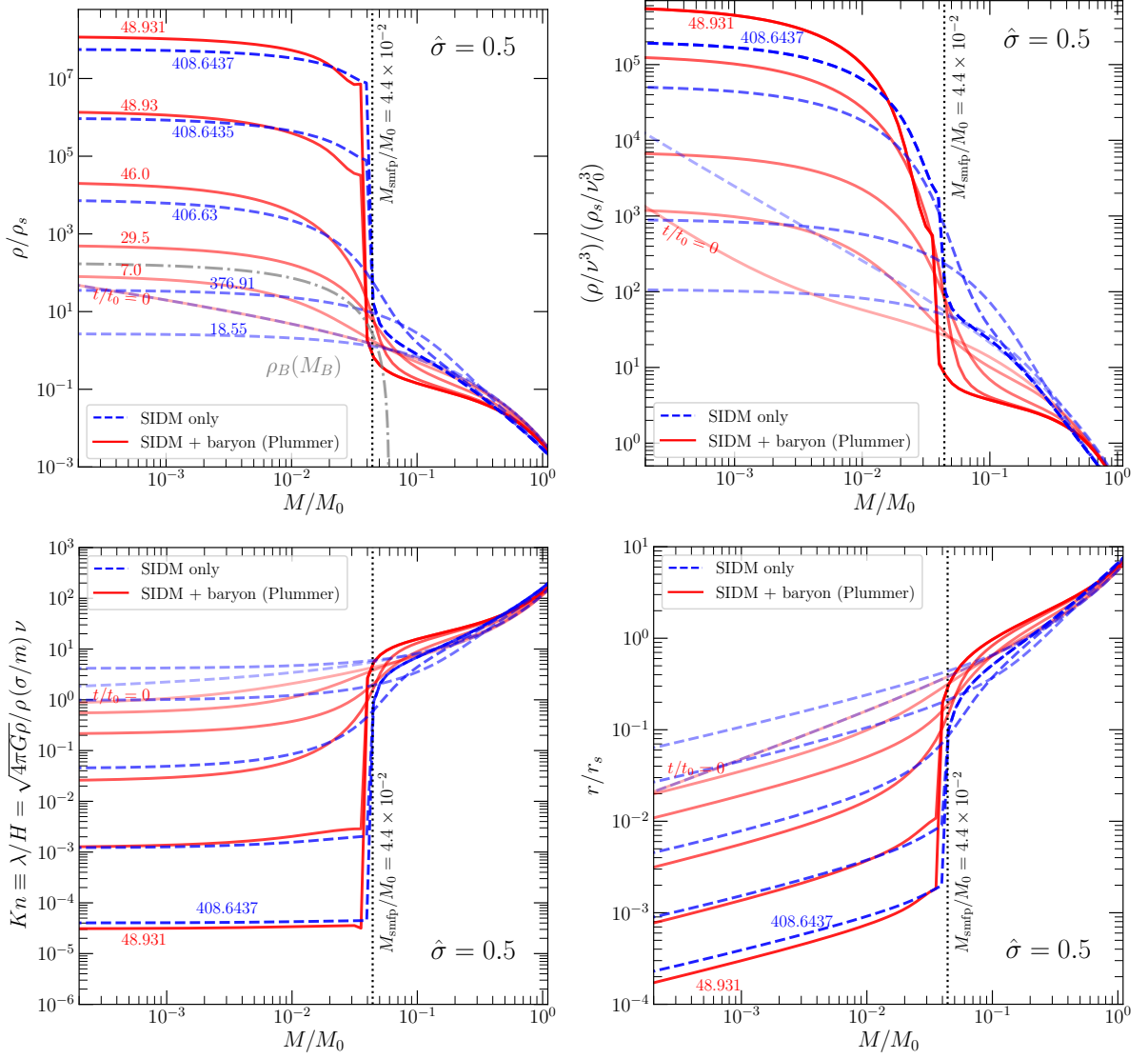


FIG. 3. Evolution profiles for $\hat{\sigma} = \rho_s r_s (\sigma/m) = 0.5$. Shown are the density (top left), the ratio ρ/ν^3 (top right), the Knudsen number (bottom left), and the radius (bottom right) as functions of enclosed mass at different stages of gravothermal collapse, with (solid red) and without (dashed blue) including the baryonic potential. The fiducial quantities are defined as $t_0 = 1/\sqrt{4\pi G \rho_s}$, $M_0 = 4\pi \rho_s r_s^3$, and $\nu_0 = r_s \sqrt{4\pi G \rho_s}$ in terms of the halo parameters ρ_s and r_s . The dotted vertical lines mark the boundary of the short mean free path region, defined by $Kn = 1$. In the top left panel, the dash-dotted curve shows the baryon density profile.

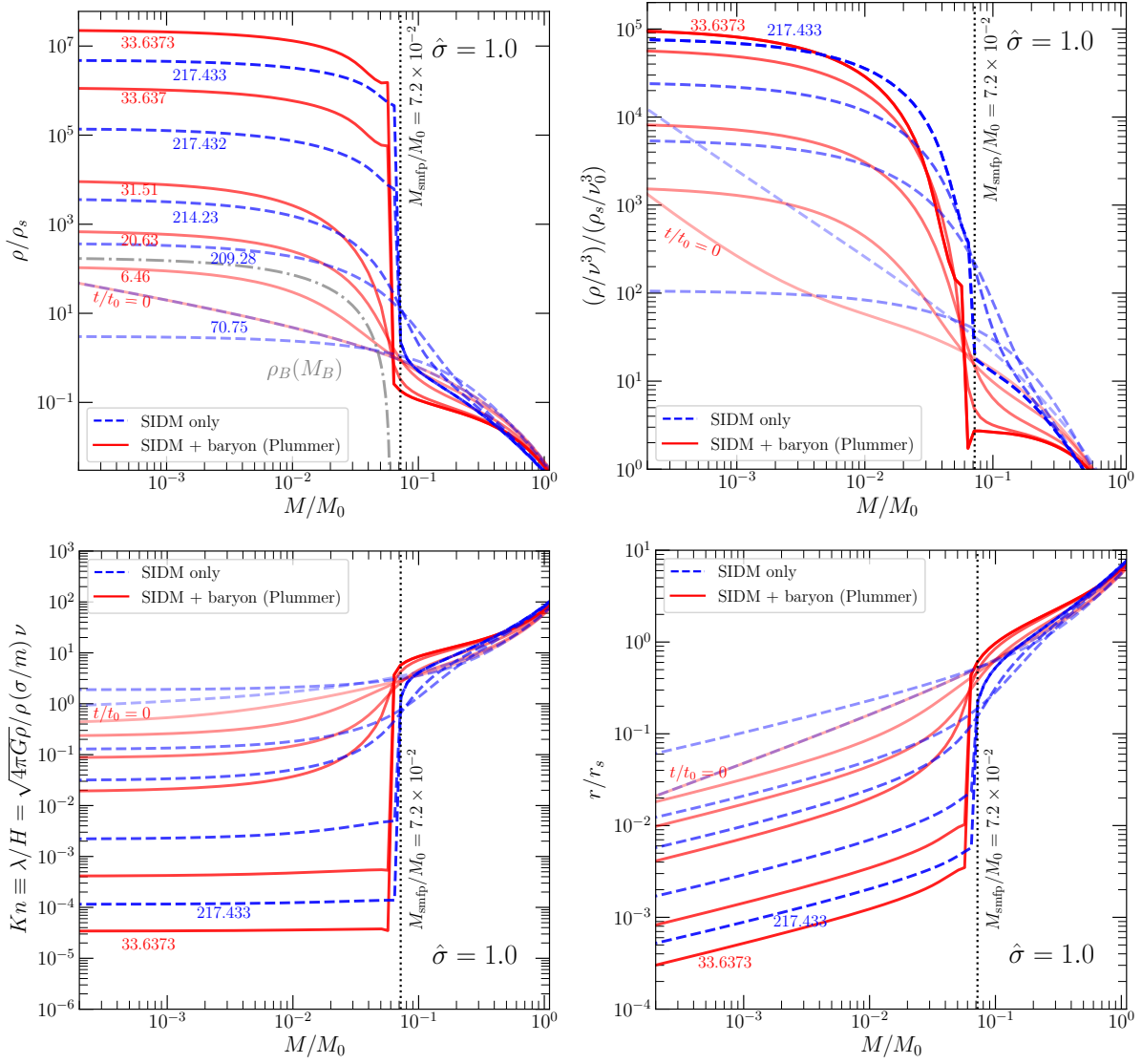


FIG. 4. Similar to Fig. 3, but for $\hat{\sigma} = (\sigma/m)\rho_s r_s = 1.0$.